Inorganic Chemistry

Article

pubs.acs.org/IC

Functionalization of Krebs-Type Polyoxometalates with N,O-Chelating Ligands: A Systematic Study

Beñat Artetxe,[†] Santiago Reinoso,*[,†] Leire San Felices,[‡] Pablo Vitoria,[†] Aroa Pache,[†] Jagoba Martín-Caballero,[†,§] and Juan M. Gutiérrez-Zorrilla*[,†,§]

[†]Departamento de Química Inorgánica, Facultad de Ciencia y Tecnología, Universidad del País Vasco UPV/EHU, P.O. Box 644, 48080 Bilbao, Spain

[‡]Servicios Generales de Investigación SGIker, Facultad de Ciencia y Tecnología, Universidad del País Vasco UPV/EHU, P.O. Box 644, 48080 Bilbao, Spain

[§]BCMaterials, Parque Científico y Tecnológico de Bizkaia, Edificio 500-1, 48160 Derio, Spain

Supporting Information

ABSTRACT: The first organic derivatives of 3d-metal-disubstituted Krebs-type polyoxometalates have been synthesized under mild bench conditions via straightforward replacement of labile aqua ligands with N,O-chelating planar anions on either preformed or in situ-generated precursors. Nine hybrid clusters containing carboxylate derivatives of five- or six-membered aromatic N-heterocycles as antenna ligands have been obtained as pure crystalline phases and characterized by elemental and thermal analyses, infrared spectroscopy, and single-crystal X-ray diffraction. They all show the general formula $[\{M^{II}L(H_2O)\}_2(WO_2)_2(B\text{-}\beta\text{-}XW_9O_{33})_2]^{n-}$ and can be classified as follows: **1-SbM**, where L = 1*H*-imidazole-4-carboxylate (imc), X = Sb^{III}, *n* = 12, and M^{II} = Mn, Co, Ni, Zn; **1-TeM**, where L = imc, X = Te^{IV}, *n* = 10, and M^{II} = Mn, Co; **2-SbNi**, where L = 1*H*-pyrazole-3-carboxylate (pzc), X = Sb^{III}, *n* = 12, and M^{II} = Ni; and **3-SbM**, where L = pyrazine-2-carboxylate (pyzc), X =Sb^{III}, *n* = 12, and M^{II} = Co, Zn. The 3d-metal-disubstituted tungstotellurate(IV) skeleton of compounds **1-TeM** is unprecedented in polyoxometalate chemistry. The stability of these hybrid Krebs-type species in aqueous solution has been confirmed by ^{1}H NMR spectroscopy performed on the diamagnetic **1-SbZn** and **3-SbZn** derivatives. Our systematic study of the reactivity of disubtituted Krebs-type polyoxotungstates toward diazole-, pyridine-, and diazinecarboxylates demonstrates that organic derivatization is strongly dependent on the nature of the ligand, as follows: imc displays a "universal ligand" character, as functionalization takes place regardless of the external 3d metal and heteroatom; pzc and pyzc show selectivity toward specific 3d metals; pyridazine-3-carboxylate and pyrimidine-4-carboxylate promote partial decomposition of specific precursors, leading to $[M^{II}L_2(H_2O)_2]$ complexes; and picolinate is inert under all conditions tested.

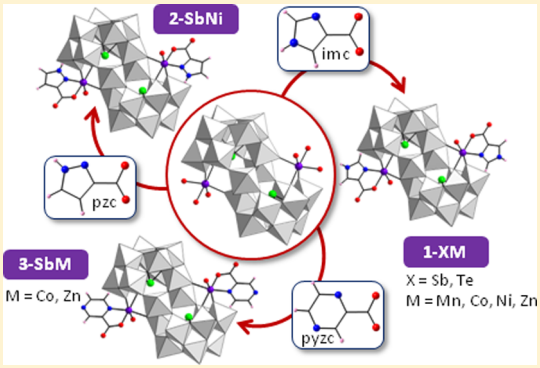

INTRODUCTION

Polyoxometalates (POMs) are anionic metal−oxygen clusters with unique structural variety and potential applications in fields such as catalysis, medicine, magnetism, and materials science.[1] Derivatization of POMs with additional organic functions represents one of the most relevant topics in the field at present. The resulting hybrids have been identified as a key factor for POM clusters to be suitably incorporated into polymeric materials or carbon nanotubes, firmly anchored on diverse surfaces (e.g., oxides, metals, graphite), or even to interact with metallic nanoparticles.[2] The use of tailored POM hybrids for constructing such composites might pave the way for new multifunctional devices like immobilized catalysts or photoactive systems for energy conversion and storage. However, this usually requires elaborate organic functions that can be achieved only via multistep synthetic work on so-called preformed hybrid POM platforms.[3]

Different approaches have been applied to prepare solution-stable hybrid POMs on a precursor scale. One of the most extensively explored routes consists in combining lacunary Keggin or Wells−Dawson polyoxotungstates with p-block organoderivatives such as organosilyl, -germyl, -phosphoryl, or -stannyl moieties.[4] Another elegant strategy to covalently attach organic groups to POM skeletons involves replacement of shell O atoms with O- or N-donor ligands, as exemplified by the series of tris(alkoxo)-capped Anderson−Evans, hexavanadate, or $[H_4P_2V_3W_{15}O_{62}]^{5-}$ anions and also by the different organoimido or -diazenido derivatives of Lindqvist-type molybdates reported to date.[5]

Several groups, including ours, have studied the synthesis of hybrid species via grafting of transition-metal complexes on

Received: September 15, 2014
Published: November 14, 2014

   dx.doi.org/10.1021/ic502232v | *Inorg. Chem.* 2015, 54, 241−252

POM surfaces.[6] However, the limited control of the anchoring positions is a major drawback in terms of predictability and applicability. Nevertheless, this might be overcome by using suitable d- or f-metal-substituted POMs with exposed metal centers to replace labile molecules in their coordination spheres (e.g., water, acetate anions) with functional organic ligands. Examples are less abundant[7] because steric effects and the repulsion between anionic ligands and POMs can make straightforward complexation of these centers certainly challenging, in such a way that large ligand excesses and harsh synthetic conditions are often required. Even if complexation is successful, crystallization of the hybrid species can also entail difficulties due to hydrolysis of weak metal-to-ligand bonds, which is often associated with monodentate N-donor groups. The coordinative strategy can be improved by combining ligands with polydentate character and POM assemblies that contain polynuclear d- or f-metal arrays with accessible coordination sites in close vicinity. Related reports include, for example, the embedding of metal chelates within different POM fragments, the transfer of chirality from enantiomerically pure tartrate to a Zr^{IV}-containing POM, the development of a general method for grafting functional carboxylates to polysubstituted trilacunary Keggin fragments, and the use of Ni_6-containing POMs stabilized by diamines to construct molecular cages or porous frameworks.[8]

Transition-metal-substituted Krebs-type POMs could be ideal candidates for performing such ligand replacements because (i) they show 6−10 accessible water molecules, (ii) they are stable in solution over a wide pH range and can be prepared in large amounts, and (iii) their structure allows systematic compositional variations to be carried out. The parent $[\{WO_2(OH)\}_2(WO_2)_2(XW_9O_{33})_2]^{n-}$ sandwich-type cluster consists of two trilacunary $\{B\text{-}\beta\text{-}XW_9\}$ Keggin subunits linked by two inner *cis*-$\{WO_2\}$ and two outer *fac*-$\{WO_2(OH)\}$ octahedral groups.[9] As indicated by Krebs and co-workers for the tungstoantimonate(III) derivative, the latter groups are labile, allowing defect $[(WO_2)_2(XW_9O_{33})_2]^{(n+2)-}$ intermediates to be formed in solution and stabilized by incorporation of different electrophiles at the vacant external positions. A defect Krebs-type anion with dimethyl sulfoxide (DMSO)-coordinated inner tungsten atoms was indeed reported some years ago by Bi et al.[10] Exchange of the outer $\{WO_2(OH)\}$ groups for $\{M(H_2O)_3\}$ moieties has been thoroughly studied, resulting in a large family of 3d-metal-disubstituted $[\{M(H_2O)_3\}_2(WO_2)_2(XW_9O_{33})_2]^{n-}$ Krebs-type species with M = Mn^{II}, Fe^{III}, Co^{II}, Ni^{II}, or Zn^{II} and X = Sb^{III} or Bi^{III}.[9,11] Moreover, the inner positions have also been fully or partially exchanged for $\{M(H_2O)_2\}$ groups in several tri- and tetrasubstituted analogues, specially for certain heteroatoms (X = As^{III}, Te^{IV}, Se^{IV}) or trivalent metals (M = Fe^{III}, Cr^{III}, Al^{III}, In^{III}).[12] Attempts to introduce other functional electrophiles at external positions include the catalytically active $\{Ru^{IV}_4O_6(H_2O)_9\}^{4+}$ fragment, photoactive $\{M(CO)_3\}^{3+}$ (M = Re^{III}, Mn^{III}) moieties, organoruthenium or -tin groups, or even rare-earth metals.[13]

Some Krebs-type clusters have shown catalytic activity in microwave-assisted oxygenation of cyclohexane, bioinspired oxidation of catechols, epoxidation of dienes, and photosensitized water oxidation processes and even as Lewis acid catalysts.[11a,12e,14] Despite these interesting properties and their obvious potential as molecular precursors in ligand replacement reactions, the organic functionalization of 3d-metal-substituted Krebs-type POMs has remained largely unexplored, as pointed out by Dolbecq and co-workers[2d] in a recent review. Besides a few DMSO-coordinated species,[15] only the oxalate derivatives $[Fe^{III}_4(ox)_4(H_2O)_2(X^{III}W_9O_{33})_2]^{14-}$ (X = As, Sb, Bi) can be found in the literature to our knowledge.[14c,16] However, these species might not be representative models for the formation of hybrid Krebs-type clusters because the oxalate anion is a peculiar O-donor ligand with very specific coordinating features and the reactivity of a given Fe^{III}-containing POM is often hardly comparable to that of its M^{II}-substituted analogue.

Encouraged by the above, we decided to perform a systematic investigation of the reactivity of 3d-metal-substituted Krebs-type POMs as precursors for the preparation of molecular hybrid clusters via classical coordination chemistry under mild synthetic conditions. We focused our studies on the family of disubstituted $[\{M^{II}(H_2O)_3\}_2(WO_2)_2(Sb^{III}W_9O_{33})_2]^{10-}$ tungstoantimonates (M^{II} = Mn, Co, Ni, Zn), and after considering that previous attempts involving aliphatic N,N-donor ligands such as ethylenediamine did not prove to be successful,[16] we first tested some planar N,O-chelating ligands. Carboxylate derivatives of five- and six-membered N-donor heterocycles were selected for our purpose, and more specifically, diazole-, pyridyl-, and diazinecarboxylates. Here we report a series of solution-stable $[\{M^{II}L(H_2O)\}_2(WO_2)_2(Sb^{III}W_9O_{33})_2]^{12-}$ anions that constitute the first organic derivatives of disubstituted Krebs-type POMs to date. They can be classified as follows: **1-SbM**, where L = 1*H*-imidazole-4-carboxylate (imc) and M^{II} = Mn, Co, Ni, Zn; **2-SbNi**, where L = 1*H*-pyrazole-3-carboxylate (pzc) and M^{II} = Ni; and **3-SbM**, where L = pyrazine-2-carboxylate (pyzc) and M^{II} = Co, Zn. Moreover, in the course of our studies we were also able to obtain the $[\{M^{II}(imc)(H_2O)\}_2(WO_2)_2(Te^{IV}W_9O_{33})_2]^{10-}$ analogues (**1-TeM**, M^{II} = Mn, Co) as pure crystalline phases and some mononuclear complexes of general formula $[M^{II}L_2(H_2O)_2]$. The 3d-metal-disubstituted tungstotellurate(IV) skeleton of **1-TeM** is unprecedented in POM chemistry.

EXPERIMENTAL SECTION

Materials and Methods. $Na_9[Sb^{III}W_9O_{33}]$ was synthesized according to literature procedures,[9] whereas the sodium salts $Na_{10}[\{M^{II}(H_2O)_3\}_2(WO_2)_2(Sb^{III}W_9O_{33})_2]\cdot 40H_2O$ (M^{II} = Mn, Co, Ni, Zn) were prepared following the method reported by Piepenbrink et al. for the Mn^{II} species.[11d] All of the POM precursors were identified by infrared spectroscopy. All other reagents were purchased from commercial sources and used without further purification. Carbon, nitrogen, and hydrogen were determined on a PerkinElmer 2400 CHN analyzer, whereas metal analyses were performed on a Q-ICP-MS ThermoXSeries II analyzer. Fourier transform infrared (FT-IR) spectra were recorded on KBr pellets using a Shimadzu FTIR-8400S spectrophotometer. Solution ^{1}H NMR spectra were measured on a Bruker AVANCE 500 spectrometer (D_2O, 500 MHz, one-bay).

General Synthetic Procedures. Three different synthetic methods were evaluated:

Method 1. To a hot solution of $Na_2WO_4\cdot 2H_2O$ (1.32 g, 4.0 mmol) in aqueous 1 M acetic acid/sodium acetate buffer (40 mL) were added successively the heteroatomic source (0.40 mmol; $SbCl_3$, 91 mg; TeO_2, 64 mg) dissolved in aqueous 6 M HCl (1 mL) and the corresponding 3d metal salt (0.40 mmol; $MnCl_2\cdot 4H_2O$, 79 mg; $CoCl_2\cdot 6H_2O$, 95 mg; $NiCl_2\cdot 6H_2O$, 95 mg; $Zn(NO_3)_2\cdot 6H_2O$, 119 mg). After 20 min of stirring at 90 °C, 1*H*-imidazole-4-carboxylic acid (44 mg, 0.40 mmol) was added, and the resulting mixture was kept for 1 h at 90 °C, cooled to room temperature, and filtered to remove any insoluble residue.

Method 2. To a hot solution of $Na_{10}[\{M^{II}(H_2O)_3\}_2(WO_2)_2(Sb^{III}W_9O_{33})_2]\cdot 40H_2O$ (M^{II} = Mn, Co, Ni, Zn; 620 mg, 0.10 mmol) in aqueous 1 M acetic acid/sodium acetate buffer (30 mL) was added the corresponding organic ligand (0.20 mmol). The resulting mixture was kept for 1 h at 90 °C, cooled to room temperature, and filtered to remove any insoluble residue.

Method 3. To a hot solution of $Na_9[Sb^{III}W_9O_{33}]\cdot 19H_2O$ (251 mg, 0.10 mmol) in aqueous 1 M acetic acid/sodium acetate buffer (30 mL)

dx.doi.org/10.1021/ic502232v | Inorg. Chem. 2015, 54, 241−252

Table 1. Crystallographic Data for 1-SbM (M = Mn, Co, Ni, Zn), 1-TeM (M = Mn, Co), 2-SbNi, and 3-SbM (M = Co, Zn)

	1-SbMn	1-SbCo	1-SbNi	1-SbZn
formula	$C_8H_{99.6}Mn_{2.4}N_4Na_{12}O_{120}Sb_2W_{19.6}$	$C_8H_{99.6}Co_{2.4}N_4Na_{12}O_{120}Sb_2W_{19.6}$	$C_{7.2}H_{97.2}N_{3.6}Na_{12}Ni_{1.8}O_{120}Sb_2W_{20.2}$	$C_{7.2}H_{97.2}N_{3.6}Na_{12}O_{120}Sb_2W_{20.2}Zn_{1.8}$
fw (g mol^{-1})	6427.2	6436.8	6493.7	6505.7
crystal system	triclinic	triclinic	monoclinic	triclinic
space group	$P\bar{1}$	$P\bar{1}$	$P2_1/c$	$P\bar{1}$
a (Å)	13.8331(4)	13.6242(7)	16.2173(3)	13.8450(4)
b (Å)	14.6798(3)	14.7481(6)	27.2085(3)	14.6579(4)
c (Å)	15.7557(5)	15.6620(9)	13.0112(2)	15.7431(4)
α (deg)	69.160(3)	68.763(5)	90	68.890(2)
β (deg)	71.318(3)	71.840(5)	108.999(2)	70.831(2)
γ (deg)	87.719(2)	87.406(4)	90	87.242(2)
V (Å^3)	2822.65(13)	2779.0(2)	5428.42(14)	2806.29(13)
Z	1	1	2	1
D_{calcd} (g cm^{-3})	3.781	3.846	3.973	3.850
μ (mm^{-1})	20.781	44.529	22.279	21.630
collected reflns	14573	18695	22924	19508
unique reflns (R_{int})	9892 (0.037)	9901 (0.068)	10647 (0.022)	11630 (0.018)
obsd reflns [$I > 2\sigma(I)$]	9096	7585	9608	10873
parameters	408	406	390	407
$R(F)^a$ [$I > 2\sigma(I)$]	0.047	0.049	0.034	0.025
$wR(F^2)^a$ (all data)	0.126	0.134	0.073	0.057
GOF	1.051	0.990	1.091	1.093

	1-TeMn	1-TeCo	2-SbNi	3-SbCo	3-SbZn
formula	$C_8H_{88}K_3Mn_2N_4Na_7O_{115}Te_2W_{20}$	$C_8H_{88.8}Co_{2.2}K_3N_4Na_7O_{115}Te_2W_{19.8}$	$C_8H_{82}K_4N_4Na_8Ni_2O_{112}Sb_2W_{20}$	$C_9H_{74}Co_2K_6N_{3.6}Na_6O_{108}Sb_2W_{20}$	$C_8H_{74.4}K_6N_{3.2}Na_6O_{109}Sb_2W_{20.4}Zn_{1.6}$
fw (g mol^{-1})	6401.1	6384.9	6405.0	6372.0	6431.1
crystal system	triclinic	triclinic	triclinic	triclinic	triclinic
space group	$P\bar{1}$	$P\bar{1}$	$P\bar{1}$	$P\bar{1}$	$P\bar{1}$
a (Å)	12.2348(3)	12.1725(4)	12.2030(4)	12.2033(4)	12.2715(3)
b (Å)	13.6081(4)	13.5660(4)	13.3843(5)	15.0427(4)	15.9492(6)
c (Å)	17.2882(4)	17.1425(5)	17.3303(4)	15.8975(5)	16.0131(5)
α (deg)	91.583(2)	91.535(3)	91.809(3)	73.220(2)	65.534(3)
β (deg)	98.057(2)	98.099(3)	99.309(2)	78.478(3)	67.844(3)
γ (deg)	106.723(2)	107.057(3)	104.266(3)	67.035(3)	78.232(2)
V (Å^3)	2722.39(11)	2672.34(14)	2699.55(15)	2560.02(13)	2637.79(14)
Z	1	1	1	1	1
D_{calcd} (g cm^{-3})	3.904	3.967	3.940	4.133	4.048
μ (mm^{-1})	22.050	22.353	22.351	23.593	23.383
collected reflns	21395	17603	20516	20315	17726
unique reflns (R_{int})	10702 (0.052)	10479 (0.040)	10597 (0.047)	10067 (0.029)	10357 (0.023)
obsd reflns [$I > 2\sigma(I)$]	9672	9517	9386	9063	9486
parameters	400	393	404	404	400
$R(F)^a$ [$I > 2\sigma(I)$]	0.052	0.048	0.059	0.035	0.038
$wR(F^2)^a$ (all data)	0.137	0.129	0.168	0.083	0.097
GOF	1.091	1.080	1.077	1.052	1.058

$^aR(F) = \sum||F_o| - |F_c||/\sum|F_o|$; $wR(F^2) = \{\sum[w(F_o^2 - F_c^2)^2]/\sum[w(F_o^2)^2]\}^{1/2}$

was added the corresponding 3d metal salt (0.30 mmol; $MnCl_2{\cdot}4H_2O$, 59 mg; $CoCl_2{\cdot}6H_2O$, 71 mg; $NiCl_2{\cdot}6H_2O$, 71 mg; $Zn(NO_3)_2{\cdot}6H_2O$, 89 mg). After 10 min of stirring at 90 °C, the corresponding organic ligand (0.20 mmol) was added. The resulting mixture was kept for 1 h at 90 °C, cooled to room temperature, and filtered to remove any insoluble residue.

$Na_{12}[\{M^{II}(imc)(H_2O)\}_2(WO_2)_2(B\text{-}\beta\text{-}Sb^{III}W_9O_{33})_2]{\cdot}44H_2O$ (1-SbM, M^{II} = Mn, Co, Ni, Zn). Compounds **1-SbM** could be isolated using any of the three methods, but the best yields were obtained by applying method 3 with 1*H*-imidazole-4-carboxylic acid as the ligand (22 mg, 0.20 mmol). Crystals suitable for X-ray diffraction were obtained by slow evaporation of the final solution at room temperature for ca. 2 weeks (final volume ca. 20 mL).

*Compound **1-SbMn**.* Orange prismatic crystals. Yield: 92 mg, 31% based on W. Anal. Calcd (Found) for $Na_{12}[\{Mn(C_4H_3N_2O_2)(H_2O)\}_2(Mn(H_2O)_2)_{0.4}(WO_2)_{1.6}(SbW_9O_{33})_2]{\cdot}44H_2O$, $C_8H_{99.6}Mn_{2.4}N_4Na_{12}O_{120}Sb_2W_{19.6}$: C, 1.50 (1.46); H, 1.56 (1.51); Mn, 2.05 (1.99); N, 0.87 (0.80); Na, 4.29 (4.51); Sb, 3.79 (4.14). IR (cm^{-1}): 1578(m), 1501(w), 1435(w), 1389(m), 1238(w), 1223(w), 1090(w), 951(s), 878(s), 831(vs), 808(sh), 775(s), 658(m), 521(w).

*Compound **1-SbCo**.* Purple prismatic crystals. Yield: 70 mg, 25% based on W. Anal. Calcd (Found) for $Na_{12}[\{Co(C_4H_3N_2O_2)(H_2O)\}_2(Co(H_2O)_2)_{0.4}(WO_2)_{1.6}(SbW_9O_{33})_2]{\cdot}44H_2O$, $C_8H_{99.6}Co_{2.4}N_4Na_{12}O_{120}Sb_2W_{19.6}$: C, 1.49 (1.55); H, 1.56 (1.34); Co, 2.20 (2.03); N, 0.87 (0.86); Na, 4.29 (3.93); Sb, 3.78 (3.29). IR (cm^{-1}): 1578(m), 1499(w), 1431(w), 1389(m), 1236(w), 1219(w), 1088(w), 949(s), 872(s), 833(vs), 806(sh), 770(s), 660(m), 521(w).

*Compound **1-SbNi**.* Pale-green prismatic crystals. Yield: 90 mg, 32% based on W. Anal. Calcd (Found) for $Na_{12}[\{Ni(C_4H_3N_2O_2)(H_2O)\}_{1.8}(W(OH)O_2)_{0.2}(WO_2)_2(SbW_9O_{33})_2]{\cdot}44H_2O$, $C_{7.2}H_{97.2}N_{3.6}Na_{12}Ni_{1.8}O_{120}Sb_2W_{20.2}$: C, 1.33 (1.50); H, 1.51 (1.35); N, 0.78 (0.81); Na, 4.25 (4.04); Ni, 1.63 (1.65); Sb, 3.75 (3.45). IR (cm^{-1}): 1576(m), 1506(w), 1431(w), 1389(m), 1238(w), 1221(w), 1088(w), 949(s), 872(s), 832(vs), 808(sh), 775(s), 658(m), 517(w).

dx.doi.org/10.1021/ic502232v | Inorg. Chem. 2015, 54, 241−252

Compound ***1-SbZn***. Colorless prismatic crystals. Yield: 118 mg, 41% based on W. Anal. Calcd (Found) for $Na_{12}[\{Zn(C_4H_3N_2O_2)(H_2O)\}_{1.8}(W(OH)O_2)_{0.2}(WO_2)_2(SbW_9O_{33})_2]\cdot 44H_2O$, $C_{7.2}H_{97.2}N_{3.6}Na_{12}O_{120}Sb_2W_{20.2}Zn_{1.8}$: C, 1.33 (1.45); H, 1.50 (1.32); N, 0.78 (0.83); Na, 4.24 (4.21); Sb, 3.74 (3.67); Zn, 1.81 (1.70). IR (cm^{-1}): 1578(m), 1500(w), 1433(w), 1389(m), 1240(w), 1223(w), 1090(w), 949(s), 876(s), 839(vs), 806(sh), 773(s), 660(m), 515(w). ^{1}H NMR (500 MHz, D_2O): δ 7.58 (s, 1H, C5−H5), 8.30 (s, 1H, C2−H2) ppm.

$K_3Na_7[\{M^{II}(imc)(H_2O)\}_2(WO_2)_2(B\text{-}\beta\text{-}Te^{IV}W_9O_{33})_2]\cdot 39H_2O$ (1-TeM, M^{II} = Mn, Co). Compounds **1-TeM** were isolated using method 1. Crystals suitable for X-ray diffraction were obtained by addition of aqueous 1 M KCl (1 mL) to the final solution followed by slow evaporation at room temperature for ca. 3 weeks (final volume ca. 15 mL).

Compound ***1-TeMn***. Orange prismatic crystals. Yield: 63 mg, 23% based on W. Anal. Calcd (Found) for $K_3Na_7[\{Mn(C_4H_3N_2O_2)(H_2O)\}_2(WO_2)_2(TeW_9O_{33})_2]\cdot 39H_2O$, $C_8H_{88}K_3Mn_2N_4Na_7O_{115}Te_2W_{20}$: C, 1.50 (1.56); H, 1.39 (1.21); K, 1.83 (1.66); Mn, 1.72 (1.73); N, 0.88 (0.81); Na, 2.51 (2.64); Te, 3.99 (3.88). IR (cm^{-1}): 1578(m), 1501(w), 1431(w), 1391(m), 1236(w), 1221(w), 1090(w), 961(s), 876(s), 837(vs), 783(s), 739(w), 691(m), 658(m), 509(w).

Compound ***1-TeCo***. Purple platelike crystals. Yield: 42 mg, 15% based on W. Anal. Calcd (Found) for $K_3Na_7[\{Co(C_4H_3N_2O_2)(H_2O)\}_2(Co(H_2O)_2)_{0.2}(WO_2)_{1.8}(TeW_9O_{33})_2]\cdot 39H_2O$, $C_8H_{88.8}Co_{2.2}K_3N_4Na_7O_{115}Te_2W_{19.8}$: C, 1.50 (1.67); H, 1.40 (1.31); Co, 2.03 (1.96); K, 1.84 (1.66); N, 0.88 (0.82); Na, 2.53 (2.69); Te, 4.00 (4.08). IR (cm^{-1}): 1578(m), 1501(w), 1433(w), 1383(m), 1236(w), 1221(w), 1096(w), 963(s), 880(s), 837(vs), 791(s), 742(w), 691(m), 660(m), 511(w).

$K_4Na_8[\{Ni^{II}(pzc)(H_2O)\}_2(WO_2)_2(B\text{-}\beta\text{-}Sb^{III}W_9O_{33})_2]\cdot 36H_2O$ (2-SbNi). Compound **2-SbNi** could be isolated using either method 2 or method 3 with 1*H*-pyrazole-3-carboxylic acid as the ligand (22 mg, 0.20 mmol), and similar yields were observed for the two methods. Green blocklike crystals suitable for X-ray diffraction were obtained by addition of aqueous 1 M KCl (1 mL) to the final solution followed by slow evaporation at room temperature for ca. 1 month (final volume ca. 10 mL). Yield: 178 mg, 61% based on W. Anal. Calcd (Found) for $K_4Na_8[\{Ni(C_4H_3N_2O_2)(H_2O)\}_2(WO_2)_2(SbW_9O_{33})_2]\cdot 36H_2O$, $C_8H_{82}K_4N_4Na_8Ni_2O_{112}Sb_2W_{20}$: C, 1.50 (1.48); H, 1.29 (1.09); K, 2.44 (2.23); N, 0.87 (0.81); Na, 2.87 (2.68); Ni, 1.88 (1.83); Sb, 3.80 (3.62). IR (cm^{-1}): 1528(w), 1053(w), 1466(w), 1385(w), 1360(m), 1246(w), 1211(w), 1119(w), 1071(w), 949(s), 872(s), 837(vs), 807(s), 775(s), 664(s), 509(w).

$K_6Na_6[\{M^{II}(pyzc)(H_2O)\}_2(WO_2)_2(B\text{-}\beta\text{-}Sb^{III}W_9O_{33})_2]\cdot nH_2O$ (3-SbM; M^{II} = Co, n = 32; M^{II} = Zn, n = 33). Compounds **3-SbM** could be isolated only by applying method 3 with pyrazine-3-carboxylic acid as the ligand (25 mg, 0.20 mmol). Addition of aqueous 1 M KCl (1 mL) to the final solution and subsequent slow evaporation at room temperature afforded crystals suitable for X-ray diffraction after ca. 3 weeks (final volume ca. 15 mL).

Compound ***3-SbCo***. Red prismatic crystals. Yield: 84 mg, 29% based on W. Anal. Calcd (Found) for $K_6Na_6[\{Co(C_5H_3N_2O_2)(H_2O)\}_{1.8}(W(OH)O_2)_{0.2}(Co(H_2O)_2)_{0.2}(WO_2)_{1.8}(SbW_9O_{33})_2]\cdot 32H_2O$, $C_9H_{74}Co_2K_6N_{3.6}Na_6O_{108}Sb_2W_{20}$: C, 1.70 (1.64); H, 1.17 (0.92); Co, 1.85 (1.91); K, 3.68 (3.77); N, 0.79 (0.83); Na, 2.16 (2.22); Sb, 3.82 (3.77). IR (cm^{-1}): 1589(m), 1525(w), 1478(w), 1422(w), 1370(m), 1184(w), 1169(w), 1059(w), 1044(w), 951(s), 876(s), 833(vs), 810(s), 766(s), 661(m), 515(w), 457(w).

Compound ***3-SbZn***. Colorless prismatic crystals. Yield: 141 mg, 49% based on W. Anal. Calcd (Found) for $K_6Na_6[\{Zn(C_5H_3N_2O_2)(H_2O)\}_{1.6}(W(OH)O_2)_{0.4}(WO_2)_2(SbW_9O_{33})_2]\cdot 33H_2O$, $C_8H_{74.4}K_6N_{3.2}Na_6O_{109}Sb_2W_{20.4}Zn_{1.6}$: C, 1.49 (1.54); H, 1.18 (1.21); K, 3.64 (3.79); N, 0.70 (0.81); Na, 2.14 (2.26); Sb, 3.78 (3.89); Zn, 1.63 (1.76). IR (cm^{-1}): 1589(m), 1528(w), 1478(w), 1420(w), 1375(m), 1184(w), 1169(w), 1059(w), 1044(w), 951(s), 874(s), 837(vs), 810(s), 768(s), 663(m), 516(w), 475(w). ^{1}H NMR (500 MHz, D_2O): δ 8.78 (s, 1H, C5−H5), 9.03 (broad, 1H, C6−H6), 9.18 (s, 1H, C3−H3) ppm.

Thermal Analyses. Thermal analyses were carried out from room temperature to 700 °C at a rate of 5 °C min^{-1} on a TA Instruments SDT 2960 thermobalance with a 150 mL min^{-1} flow of synthetic air. Table S1 in the Supporting Information summarizes the most relevant thermal data for **1-SbM** (M = Mn, Co, Ni, Zn), **1-TeM** (M = Mn, Co), **2-SbNi**, and **3-SbM** (M = Co, Zn), and their respective thermogravimetric analysis/differential thermal analysis (TGA/DTA) curves are displayed in Figure S1 in the Supporting Information. Dehydration starts at room temperature and proceeds via a continuous mass loss of endothermic nature that is completed at temperatures in the range 360−390 °C for the **1-SbM** series and around 320 °C for the Te^{IV} analogues and compound **2-SbNi**. For all of these compounds, dehydration is immediately followed by an exothermic mass loss stage originating from the combination of ligand combustion and breakdown of the oxometallic cluster, which leads to the corresponding final residues at temperatures ranging from 510 °C (**1-TeCo**) to 550 °C (**2-SbNi**). In the case of compounds **3-SbM**, release of water molecules is completed at significantly lower temperatures (265 and 290 °C for the Co and Zn derivatives, respectively), in such a way that the resulting anhydrous phases remain thermally stable up to 380 °C. These phases are amorphous according to powder X-ray diffraction analyses, evidencing that both hydration and coordination water molecules are essential to stabilize the crystal packing. The final residues formed upon ligand combustion and POM breakdown are obtained above 475 °C for **3-SbCo** and 515 °C for **3-SbZn**.

X-ray Crystallography. Crystallograpic data for compounds **1-SbM** (M = Mn, Co, Ni, Zn), **1-TeM** (M = Mn, Co), **2-SbNi**, and **3-SbM** (M = Co, Zn) are summarized in Table 1. Intensity data for all of the compounds with the exception of **1-SbCo** were collected at 100(2) K on an Agilent Technologies SuperNova diffractometer (monochromatized Mo Kα radiation, λ = 0.71073 Å) equipped with an Eos CCD detector. In the case of **1-SbCo**, collection was also carried out at 100(2) K, but the Supernova diffractometer was equipped with Cu Kα radiation (λ = 1.54184 Å) and an Atlas CCD detector. Data collections, unit cell determinations, intensity data integrations, routine corrections for Lorentz and polarization effects, and analytical absorption corrections with face indexing were performed using the CrysAlis Pro software package.[17] The structures were solved using OLEX[18] and refined by full-matrix least-squares with SHELXL-97.[19] Final geometrical calculations were carried out with PLATON[20] as integrated in WinGX.[21] Bond valence sum (BVS)[22] and continuous shape measure (CShM)[23] calculations were performed using the BVSumCalc (courtesy of Dr. M. H. Dickman) and SHAPE[24] programs, respectively.

Thermal vibrations were treated anisotropically for heavy atoms (W, Sb, Te, and 3d metals). Hydrogen atoms of the organic ligands were placed in calculated positions and refined using a riding model with standard SHELXL parameters. Tungsten and the corresponding 3d metal (M) were initially disordered over the four metal positions in the central belt of the polyoxometalate clusters (two internal and two external), and their population parameters were refined without restrictions. For **1-SbMn**, **1-SbCo**, and **1-TeCo**, negligible W populations (lower than 1%) were obtained for the external sites and partial M/W occupancies of 20/80 (**1-SbMn**), 18/82 (**1-SbCo**), and 12/88 (**1-TeCo**) were found for the internal ones. The external positions were assigned as containing exclusively M in the final refinement cycle. For **1-SbNi**, **1-SbZn**, and **3-SbZn**, the internal positions showed negligible M populations, whereas partial M/W occupancies of 89/11 (**1-SbNi**), 94/6 (**1-SbZn**), and 84/16 (**3-SbZn**) were found for the external ones. In the final step, the internal positions were refined as containing only tungsten and the occupancies of the ligand atoms were set equal to that of M. For **3-SbCo**, the external W population of about 5% was found to be almost equal to the internal Co population, whereas **1-TeMn** and **2-SbNi** were the only compounds in the series that did not show any type of crystallographic M/W disorder. Additional refinement special details are discussed in the Supporting Information.

RESULTS AND DISCUSSION

Synthetic Protocol. The reactivities of some 3d-metal-substituted Krebs-type anions toward different organic ligands were evaluated to determine (i) whether Krebs-type clusters are suitable for organic derivatization via classical coordination

dx.doi.org/10.1021/ic502232v | Inorg. Chem. 2015, 54, 241−252

Scheme 1. Synthetic Approaches for 1-SbM (M = Mn, Co, Ni, Zn), 1-TeM (M = Mn, Co), 2-SbNi, and 3-SbM (M = Co, Zn)

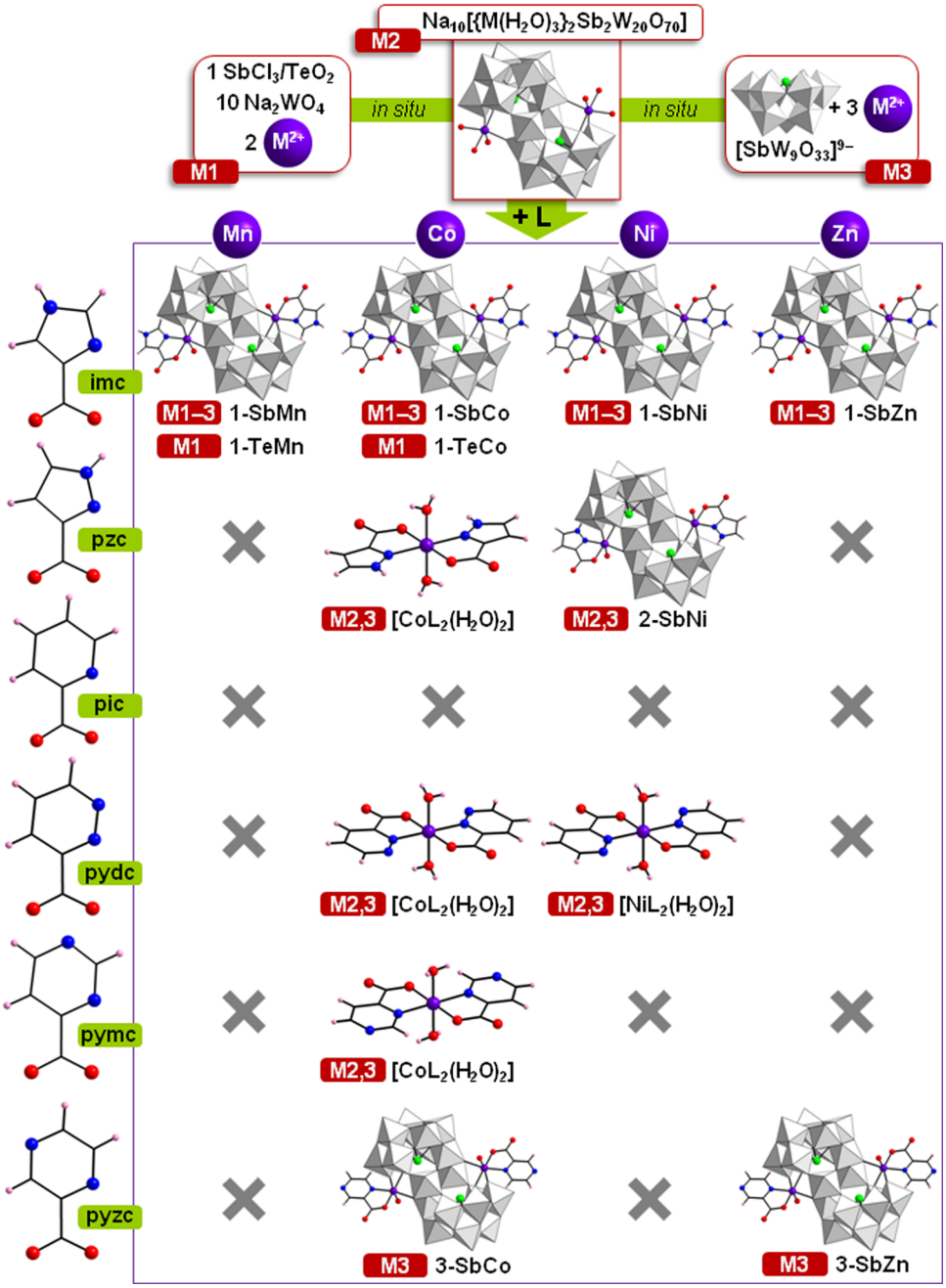

chemistry on the external 3d-metal positions under mild bench conditions and (ii) which ligand/s are the most appropriate for this purpose. We focused our studies on the $[\{M^{II}(H_2O)_3\}_2(WO_2)_2(Sb^{III}W_9O_{33})_2]^{10-}$ family of tungstoantimonates substituted with divalent 3d metals ($\mathbf{M_2Sb_2}$, M^{II} = Mn, Co, Ni, Zn). They were systematically reacted with anionic ligands having N,O-chelating capability. Planar ligands were selected for our purpose to minimize steric hindrance. Specifically, the six carboxylate derivatives of five- and six-membered N-donor aromatic heterocycles shown in Scheme 1 were selected. These are the diazolecarboxylates 1*H*-imidazole-4-carboxylate (imc) and 1*H*-pyrazole-3-carboxylate (pzc); the pyridinecarboxylate picolinate (pic); and the diazinecarboxylates pyridazine-3-carboxylate (pydc), pyrimidine-4-carboxylate (pymc), and pyrazine-2-carboxylate (pyzc).

Three synthetic methods were explored for the reaction between POMs and ligands. In all cases, hot sodium acetate-buffered medium was employed in analogy to the conditions reported by Piepenbrink et al.[11d] for the synthesis of the $\mathbf{Mn_2Sb_2}$ and $\mathbf{Zn_2Sb_2}$ anions. Method 1 consists of a one-pot reaction involving the most basic metallic reagents that can lead to the desired POM cluster (sodium tungstate, a 3d-metal chloride or nitrate, and a heteroatomic source such as $SbCl_3$) and the corresponding ligand in the stoichiometric ratio ($10WO_4^{2-}$:$1M^{2+}$:$1Sb^{III}$:1L). Method 2 is the direct stoichiometric reaction between the ligand and the sodium salt of the preformed $\mathbf{M_2Sb_2}$ precursor (M_2Sb_2:2L). In method 3, an excess of the ligand is reacted with the precursor generated in situ following literature procedures based on the trilacunary [B-α-$Sb^{III}W_9O_{33}]^{9-}$ species[11d] but with a 2-fold excess of the 3d-metal

dx.doi.org/10.1021/ic502232v | *Inorg. Chem.* 2015, 54, 241−252

salt ($[SbW_9O_{33}]^{9-}$:$3M^{2+}$:2L). All three methods were initially evaluated using the imc ligand, whereas for the rest of the organic molecules only methods 2 and 3 were tested after they were identified as the most suitable (see below). The imc ligand was also used to gain further insight into the influence of the heteroatom on the reactivity of the Krebs-type anions by replacing Sb^{III} with Te^{IV} in method 1. The reactions were monitored by IR spectroscopy on any solid material obtained by slow evaporation of the final solutions at room temperature until dryness. This technique proved to be excellent for determining the success of our functionalization attempts.

The use of four different tungstoantimonate precursors, six different N,O-chelating ligands, three different synthetic methods for imc, and two methods for the remaining five ligands resulted in 52 possible synthetic combinations. All of them were explored, and the results are summarized in Scheme 1. In addition, the results obtained with Te^{IV} as the heteroatom are also included. Reactions between Krebs-type anions and ligands were observed in 24 out of the 52 possible combinations. In the remaining 28, the only solid products isolated from the reaction mixtures were pristine Krebs-type POMs, as shown by IR spectroscopy. The 24 cases in which reaction took place can be divided into two groups according to the final product: in 16 of these reactions, organic functionalization was successful and the corresponding hybrid clusters were isolated, whereas in the remaining eight combinations the POM precursor underwent partial decomposition upon ligand attack and the corresponding $[M^{II}L_2(H_2O)_2]$ complexes were obtained. As a result, seven organic derivatives of disubstituted Krebs-type tungstoantimonates and two tunsgtotellurate analogues were isolated as pure crystalline phases. These are $[\{M^{II}(imc)(H_2O)\}_2(WO_2)_2(Sb^{III}W_9O_{33})_2]^{12-}$ (**1-SbM**, M^{II} = Mn, Co, Ni, Zn), $[\{M^{II}(imc)(H_2O)\}_2(WO_2)_2(Te^{IV}W_9O_{33})_2]^{10-}$ (**1-TeM**, M^{II} = Mn, Co), $[\{Ni(pzc)(H_2O)\}_2(WO_2)_2(Sb^{III}W_9O_{33})_2]^{12-}$ (**2-SbNi**), and $[\{M^{II}(pyzc)(H_2O)\}_2(WO_2)_2(Sb^{III}W_9O_{33})_2]^{12-}$ (**3-SbM**, M^{II} = Co, Zn). Moreover, four monomeric complexes were also obtained in the course of our studies: $[Co(pzc)_2(H_2O)_2]$ (**Co-pzc**), $[M(pydc)_2(H_2O)_2]\cdot 2H_2O$ (**M-pydc**, M = Co, Ni), and $[Co(pymc)_2(H_2O)_2]\cdot 2H_2O$ (**Co-pymc**).

Reactions with the Ligand imc. We started our investigations from ligand imc, and the complete series of **1-SbM** anions were directly obtained in the first attempt by following method 1, as identified by IR spectroscopy (Figure S2 in the Supporting Information). X-ray diffraction analyses performed on these crystals allowed us to locate the ligand coordinated to the Krebs-type framework, but unfortunately, severe disorder in the outer positions with W populations of ca. 22% prevented imc from being satisfactorily modeled. As indicated by Krebs and co-workers,[9] the intermediate $[(WO_2)_2(Sb^{III}W_9O_{33})_2]^{14-}$ can be stabilized by either two external $\{WO_2(OH)\}$ or $\{M^{II}(H_2O)_3\}$ moieties, and this competition often leads to crystallographic disorder arising from cocrystallization of plenary and disubstituted species. We tried to overcome this disorder by using an excess of M^{II} ($10WO_4^{2-}$:$2M^{2+}$:$1Sb^{III}$:1L), but the results were analogous, and therefore, we decided to explore the other two synthetic approaches.

The more rational strategy of performing a straightforward ligand replacement on the preformed cluster (method 2) also afforded crystalline **1-SbM** samples with external W populations above 20%, as in method 1. Fortunately, we could prepare the complete **1-SbM** series with trivial W occupancies in the outer positions by applying method 3. The 2-fold excess of 3d metal we used in this method proved to be essential to overcome the severe M^{II}/W disorder in the central belt of the sandwich POM skeleton. Not surprisingly, the well-known $[\{Cu(H_2O)\}_3(B\text{-}\alpha\text{-}SbW_9O_{33})_2]^{12-}$ Hervé-type POM[25] was isolated when Cu^{II} was tested in method 3 as a result of the specific coordination requirements of this metal ion. Thus, the diazolecarboxylate anion imc serves as a "universal" ligand toward disubstituted Krebs-type tungstoantimonates because (i) coordination takes place with retention of the sandwich-type framework regardless of the divalent 3d metal present in the external sites and (ii) functionalization is easily achieved in moderate to good yields regardless of the synthetic method applied, although best X-ray-quality crystals were obtained via method 3.

Taking advantage of the universality of the imc ligand as a derivatizing agent, we also explored the influence of a change in the charge of the heteroatom on the reactivity. For this purpose, we replaced $SbCl_3$ with TeO_2 as the heteroatom source in method 1 and performed an additional set of reactions. Those involving Mn or Co led to pure crystalline phases of the corresponding **1-TeMn** and **1-TeCo** hybrid analogues, which represent the first observation of a 3d-metal-disubstituted Krebs-type framework with Te^{IV} as the heteroatom. To date, only tri- and tetrasubstituted tungstotellurates(IV) have been reported in the literature.[12a,b] Crystals suitable for X-ray diffraction were obtained only upon addition of K^+ as a counterion, but in contrast to the tungstoantimonate system, the clusters did show negligible M^{II}/W disorder at the external sites, allowing satisfactory modeling of the antenna ligand.

In the case of Ni, we were able to identify the presence of the **1-TeNi** species by IR spectroscopy (Figure S3 in the Supporting Information) and to confirm its existence by single-crystal X-ray diffraction.[26] However, the bulk solid appeared to be a mixture with the bluish $[Ni(imc)_2(H_2O)_2]$ complex[27] (**Ni-imc**) and an unidentified Ni-containing all-inorganic tungstotellurate rather than a pure phase according to elemental and thermal analyses. We could manually remove the **Ni-imc** complex from the bulk, but similar greenish colors and crystal morphologies prevented us from separating pure samples of the two Ni-containing POMs. When Zn was used, batches of poorly diffracting colorless crystals were isolated, for which no evidence of organic derivatization was detected according to the absence of representative signals of the imc ligand in the organic IR region (Figure S3 in the Supporting Information).

Reactions with Other N,O-Chelating Ligands. We extended this study to the remaining five N,O-chelating ligands shown in Scheme 1, but considering the crystallographic disorder described above for method 1, we limited our evaluation to methods 2 and 3. Method 2 was kept as a control experiment to check whether formation of a given hybrid cluster was due to ligand replacement or proceeded via encapsulation of a metal chelate by a defect intermediate. In contrast to what the results afforded by imc could suggest, we found that the organic derivatization of Krebs-type anions is not trivial. Functionalization turned out to be extremely dependent on the specific nature of the ligand, and we could isolate only three additional hybrids. The following behaviors were observed for the various ligands:

(i) Diazolecarboxylates showed completely different reactivities upon modification of the relative positions of the N atoms in the ring. In contrast to the "universal" character of imc, the ligand pzc was found to be selective toward the functionalization of Ni_2Sb_2. The hybrid species **2-SbNi** was obtained as a cottony solid regardless of the synthetic method, but we could grow single crystals by addition of K^+ as a crystallizing agent. The

dx.doi.org/10.1021/ic502232v | Inorg. Chem. 2015, 54, 241−252

reactivity of pzc toward other M_2Sb_2 anions was either nonexistent or resulted in partial decomposition of the Co_2Sb_2 cluster, leading to crystalline mixtures of the precursor and the corresponding **Co-pzc** complex, as shown by IR spectroscopy (Figure S4 in the Supporting Information) and confirmed by single-crystal X-ray diffraction. This species and the **Ni-pzc** derivative were separately synthesized[28] for comparative purposes (see IR Spectroscopy below), and a brief discussion of their thermal and structural features is given in the Supporting Information. Both compounds are isostructural to the recently reported analogue $[Zn(pzc)_2(H_2O)_2]$.[29]

(ii) An archetypical chelating ligand like the pic anion proved to be fully inert toward disubstituted Krebs-type tungstoantimonates under all of the synthetic conditions tested.

(iii) As observed for pzc, the diazinecarboxylate anions pydc and pymc promoted partial decomposition of certain M_2Sb_2 POMs, resulting in mixtures of the precursors and the corresponding $[M^{II}L_2(H_2O)_2]$ monomeric complexes. This was obsered for the Co- and Ni-containing POMs in the case of pydc and only for Co_2Sb_2 when pymc was used (Figure S4 in the Supporting Information). We previously reported the structure of **Co-pydc** elsewhere.[30] The full characterization of this species, the isostructural complex **Ni-pydc**,[31] and the **Co-pymc** complex[32] (isostructural to the reported Zn and Ni analogues)[33] can be found in the Supporting Information.

(iv) The third diazinecarboxylate anion (pyzc) did not lead to complexes but rather behaved as a selective agent for the derivatization of Co_2Sb_2 and Zn_2Sb_2. The resulting hybrid derivatives were exclusively obtained via method 3 and needed the presence of K^+ to crystallize. Therefore, the direct replacement reaction on preformed precursors is not operative for this specific ligand, and the formation of **3-SbM** species must proceed through trapping of the corresponding metal chelate by a transient defect intermediate.

From the point of view of the M_2Sb_2 precursors, the stability of the parent disubstituted Krebs-type framework differs significantly from Mn to Zn. The Mn_2Sb_2 anion appears to be the most stable precursor, as it reacts only with imc to give the corresponding hybrid derivative. On the contrary, the Co_2Sb_2 cluster can be seen as the most labile because it reacts with all of the ligands except for pic, resulting in hybrid derivatives with imc and pyzc or in partial decomposition and consequent formation of $[M^{II}L_2(H_2O)_2]$ complexes for pzc, pymc, and pydc. In regard to synthetic aspects, it is also worth mentioning that crystalline side products were isolated for those failed attempts involving the Mn_2Sb_2 and Zn_2Sb_2 anions when the volume of the solutions was concentrated to the minimum. These consisted of chains of Krebs-type POMs linked via M−O−M bridges involving only the outer positions[34] and could be identified in the IR spectrum by a remarkable increase in the intensity of the central line of the ν(M−O−M) triplet with vanishing of the two side signals (Figure S5 in the Supporting Information). Related Krebs-type polymers are based on M−O−W linkages involving the $\{(WO_2)_2(SbW_9O_{33})_2\}$ fragment.[35]

IR Spectroscopy. Functionalization could be unequivocally determined by IR spectroscopy prior to single-crystal X-ray studies, making this simple technique a powerful tool to confirm the existence of hybrid Krebs-type species. As an illustrative example, the spectrum of **1-SbCo** (Figure 1) shows a series of weak- to medium-intensity peaks in the organic 1090−1580 cm^{-1} range that evidence the presence of the imc anion, whereas the POM domain below 1000 cm^{-1} closely resembles that of the precursor with negligible variations in the band positions except

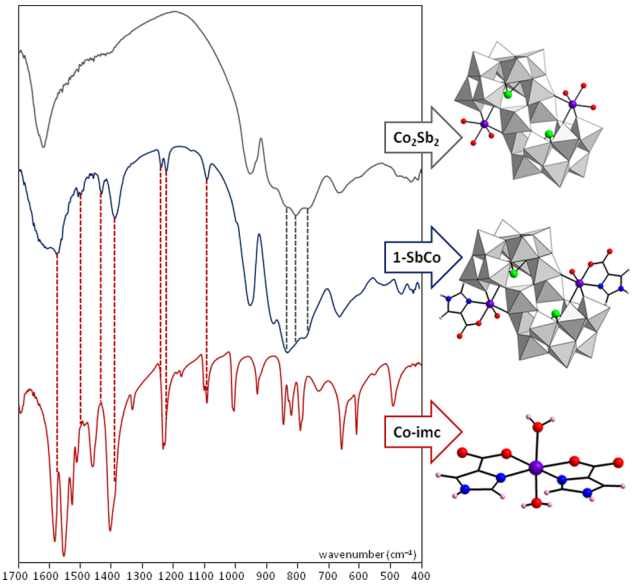

Figure 1. Infrared spectrum of **1-SbCo** compared with those of its Co_2Sb_2 precursor and the **Co-imc** complex. The fingerprint of the POM functionalization is highlighted with dotted lines.

for a ca. 10 cm^{-1} red shift in the signal associated with the ν(Co−O) mode (~670 cm^{-1}).[36] This fact indicates retention of the sandwich metal−oxo framework upon reaction. However, remarkable differences are observed when this spectrum is compared with those of the Co_2Sb_2 precursor and the $[Co(imc)_2(H_2O)_2]$ complex (**Co-imc**) with imc ligands in the same coordinating fashion.[37] In the organic region, several bands are significantly displaced with respect to the spectrum of **Co-imc**, especially those above 1400 cm^{-1}, which are mainly related to stretching vibrations in the imidazole ring and N−H bending. In the POM domain, the triplet of signals originating from the M−O−M stretching (840−765 cm^{-1}) undergoes a clear change in relative intensities compared with those of Co_2Sb_2, in such a way that the central peak becomes almost shadowed by an increase in the intensity of the left line. Both types of modifications were systematically observed for all of the hybrid Sb^{III} anions (Figure S6 in the Supporting Information), and hence they must represent inherent signals of the organic derivatization of the Krebs-type framework. This fingerprint allowed us to discriminate between homogeneous solid phases of functionalized clusters and those mixtures of pristine M_2Sb_2 precursors with $[M^{II}L_2(H_2O)_2]$ complexes mentioned above (**Co-pzc**, **Co-pydc**, **Ni-pydc**, and **Co-pymc**), whose spectra are merely the result of the overlap of the individual profiles of the two components.

Molecular Structures. All of the **1-XM**, **2-SbNi**, and **3-SbM** hybrid POMs retain the parent 3d-metal-disubstituted Krebs-type skeleton upon derivatization. This is composed of two trilacunary Keggin $[B\text{-}\beta\text{-}Sb^{III}W_9O_{33}]^{9-}$ subunits linked via corner sharing by two internal WO_6 octahedra (each showing two cis-related terminal O atoms) and two M^{II} atoms coordinated at external positions to three terminal O_{POM} atoms in relative *fac* arrangement that belong to a $\{W_2O_{11}\}$ corner-shared fragment of one subunit (O5M/O7M) and to the 60°-rotated $\{W_3O_{13}\}$ trimer of the second subunit (O1T). The polyanions **1-SbNi**, **1-SbZn**, and **3-SbZn** display relatively low W populations of 11, 6, and 16% in their respective external positions. For **1-SbMn**, **1-SbCo**, and **1-TeCo** containing the more oxophilic 3d metals, there is no crystallographic W/M^{II} external disorder, but we

dx.doi.org/10.1021/ic502232v | Inorg. Chem. 2015, 54, 241−252

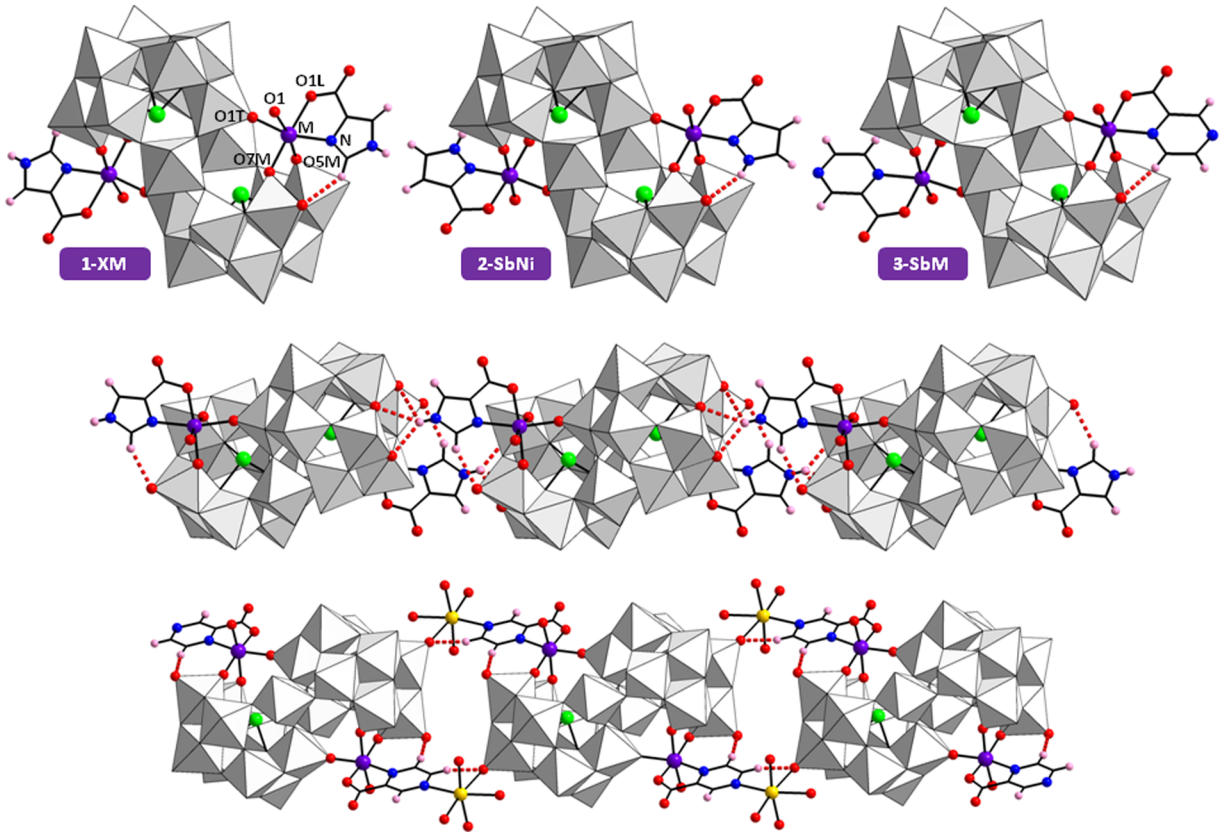

Figure 2. (top) Molecular structures of the hybrid Krebs-type clusters **1-SbM** (M = Mn, Co, Ni, Zn), **1-TeM** (M = Mn, Co), **2-SbNi**, and **3-SbM** (M = Co, Zn), together with atom labeling. (middle) Hydrogen-bonded POM chain in the crystal packing of **1-SbM** (M = Mn, Co, Zn). (bottom) Sodium-mediated one-dimensional POM assembly in the crystal packing of **3-SbZn**. Color code: WO_6, gray octahedra; Sb or Te, green; 3d metal, violet; O, red; N, blue; H, pink; Na, yellow; C−H···O and N−H···O interactions, dotted red lines.

Table 2. Bond Lengths (Å) and Continuous Shape Measures (CShM)[a] for the $M^{II}O_5N$ Chromophores of 1-SbM (M = Mn, Co, Ni, Zn), 1-TeM (M = Mn, Co), 2-SbNi, and 3-SbM (M = Co, Zn) Compared with Those of the Corresponding $[M^{II}L_2(H_2O)_2]$ Complexes (M-L) and $[\{M^{II}(H_2O)_3\}_2(WO_2)_2(Sb^{III}W_9O_{33})_2]^{10-}$ Precursors (M_2Sb_2)[b]

complex	M−O1L	M−N	M−O1	M−O5M	M−O7M	M−O1T	CShM	ref
Mn_2Sb_2			2.18(4)	2.10(4)	2.16(3)	2.18(4)	0.422	11d
1-SbMn	2.194(9)	2.241(11)	2.236(12)	2.155(9)	2.122(9)	2.150(9)	1.015	this work
1-TeMn	2.183(11)	2.203(11)	2.206(11)	2.149(10)	2.154(10)	2.148(9)	1.033	this work
Co_2Sb_2			2.060(14)	2.065(10)	2.037(12)	2.106(12)	0.383	11c
1-SbCo	2.095(12)	2.107(13)	2.137(13)	2.096(10)	2.068(10)	2.078(12)	0.627	this work
1-TeCo	2.067(10)	2.117(11)	2.097(11)	2.099(9)	2.071(10)	2.087(10)	0.824	this work
Co-imc	2.177(1)	2.076(2)						37
3-SbCo	2.029(8)	2.153(10)	2.107(7)	2.089(7)	2.060(6)	2.096(8)	1.130	this work
Co-pyzc	2.088(2)	2.095(2)						38
Ni_2Sb_2			2.07(2)	2.012(18)	2.004(17)	2.042(15)	0.224	11e
1-SbNi	1.996(8)	2.022(10)	2.079(8)	2.069(7)	2.074(7)	2.074(7)	0.510	this work
Ni-imc	2.076(1)	2.050(2)						27
2-SbNi	2.049(13)	2.028(16)	2.091(13)	2.057(12)	2.028(12)	2.047(12)	0.537	this work
Ni-pzc	2.074(1)	2.067(2)						this work
Zn_2Sb_2			2.095(13)	2.052(12)	2.110(10)	2.107(10)	0.241	11d
1-SbZn	2.098(6)	2.091(5)	2.110(6)	2.120(5)	2.043(5)	2.146(5)	0.815	this work
Zn-imc	2.163(1)	2.075(2)						39
3-SbZn	2.022(9)	2.065(12)	2.067(10)	2.112(8)	2.069(8)	2.127(9)	0.938	this work
Zn-pyzc	2.10(2)	2.080(2)						38

[a]Using the ideal octahedron as the reference shape. [b]For the atom labeling, see Figure 2.

found noticeable M^{II} occupancies at the internal positions (20, 18, and 12%, respectively). For comparison, Krebs reported external W occupancies of 9 and 20% for **Mn_2Sb_2** and **Zn_2Sb_2**,[11d] while Niu observed internal W/M^{II} disorders for **Mn_2Sb_2** and **Co_2Sb_2** that compare well to ours.[12d]

dx.doi.org/10.1021/ic502232v | Inorg. Chem. 2015, 54, 241−252

The octahedral coordination spheres of the M^{II} centers are completed with one water molecule (O1) and one O,N-chelating ligand. BVS calculations confirm the O1 water molecule to be the only protonation site, and the relatively low values obtained for the terminal O atoms of the internal positions in **1-SbMn**, **1-SbCo**, and **1-TeCo** (1.39−1.51) are in agreement with the above-mentioned W/M^{II} disorder. The arrangement of the antenna ligand constitutes a common structural feature in all of our hybrid clusters. The ligand anchors in such a way that the coordinating N atom and the O1T atom of the rotated trimer are *trans* to each other and the aromatic ring forms angles in the 51−58° range with the plane defined by the four metal centers of the central belt (**1-SbM**, 56−58°; **1-TeM**, 51−53°; **2Sb-Ni**, 53°; **3-SbM**, 52−55°). As shown in Figure 2, this orientation allows for establishing an intramolecular $C-H\cdots O_{POM}$ hydrogen bond ($N-H\cdots O_{POM}$ for **2-SbNi**) involving the proton located next to the coordinating N atom ($C\cdots O_{POM}$ = 3.125(10)−3.218(16) Å for **1-SbM**; 3.182(18)−3.293(18) Å for **1-TeM**; 3.256(17)−3.273(2) Å for **3-SbM**; $N\cdots O_{POM}$ = 2.998(18) Å for **2-SbNi**). There are no significant variations in the $M-O_{POM}$ bonding upon functionalization, and the M−N and $M-O_L$ bond lengths are also in agreement with those reported for complexes $[M^{II}L_2(H_2O)_2]$ (Table 2). CShM calculations show that the distortion of the M^{II} coordination spheres from the ideal octahedral geometry increases with the ionic radius and that this trend is maintained and even stressed upon functionalization as a result of the introduction of a chelating ligand with a nearly rigid bite angle.

Crystal Packing. Two different crystalline phases have been identified for the **1-SbM** sodium salts: triclinic $P\bar{1}$ (M = Mn, Co, Zn) or monoclinic $P2_1/c$ (M = Ni). In all cases, the hybrid clusters closely associate to each other in one-dimensional arrangements through trifurcated hydrogen bonds that are established between the imidazole N−H groups and the bridging O atoms of the tetrameric $\{W_4O_{18}\}$ faces (Figure 2 and Table S2 in the Supporting Information). The tilt angle of the imc ligand with respect to the plane defined by the M^{II} and Sb^{III} centers is more pronounced for monoclinic **1-SbNi** (47°) than for the triclinic analogues (33−36°), and this slightly modifies the hydrogen-bonding network, as shown in Figure S7 in the Supporting Information. Despite these subtle variations, the hybrid POM chains are virtually identical in the two types of phases, but they pack following different structural patterns depending on the crystal system: the triclinic phase shows a brick-wall motif with chains parallel to the $[0\bar{1}1]$ direction, whereas a herringbone pattern with chains propagating along the [101] direction is observed for the monoclinic one.

Hydrogen-bonded POM chains packed following a brick-wall motif are also observed in the structures of **1-TeM** and **2-SbNi**. For the former, the chains are similar to those of triclinic **1-SbM** but have considerably longer $N\cdots O_{POM}$ distances, whereas adjacent clusters are held together by trifurcated $C-H\cdots O_{POM}$ interactions instead of $N-H\cdots O_{POM}$ hydrogen bonds for the latter. The connectivity between contiguous POMs in **2-SbNi** closely resembles that found in monoclinic **1-SbNi** because the pyrazole ring adopts a nearly identical tilt angle with respect to the plane defined by the Ni/Sb atoms (47°). In the case of the **3-SbM** pair, the fact that the position of the pyz ring pointing outward is occupied by the nonchelating N atom prevents the hybrid clusters from assembling via hydrogen bonds, and this might explain the low tilt angle displayed by the ligands (25°). The crystal packing thus appears to be driven by the alkaline cations. Compound **3-SbZn** shows one-dimensional POM assemblies in which adjacent POMs are linked by two Na^+ ions coordinated to terminal O_{POM} atoms and the nonchelating N_{pyz} atoms (Figure 2), whereas the latter remain uncoordinated in **3-SbCo** and the POMs associate through the coordination sphere of the K^+ ions located in the pockets of the cluster belt (Figure S8 in the Supporting Information).

Solution Stability. In order to investigate the stability of our hybrid POMs in aqueous solution, we performed ^1H NMR studies of the diamagnetic **1-SbZn** species and compared the spectrum with those of the **Zn-imc** complex prepared as reported previously[39] and the free ligand, both in its commercial acidic form (Himc) and as the anionic carboxylate derivative (imc) generated in situ by mixing equimolar quantities of Himc and $LiOH\cdot H_2O$ (Figure 3). The spectrum of the free acidic ligand

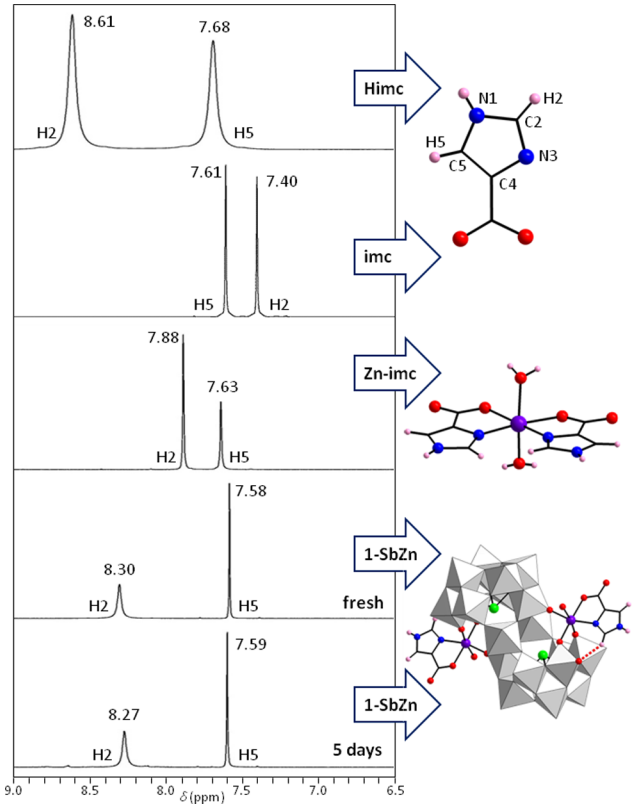

Figure 3. ^1H NMR spectrum of **1-SbZn** compared with those of 1*H*-imidazole-4-carboxylic acid (Himc), the corresponding carboxylate anion (imc), and the **Zn-imc** complex.

shows two singlets at 8.61 and 7.68 ppm that correspond to the protons located next to the coordinating N atom (H2) and to the carboxylate substituent (H5), respectively. The signals of the two nonequivalent imidazole protons undergo upfield shifts upon deprotonation of the carboxylic function due to the increase in electron density on the imidazole ring. This change in the chemical shift ($\Delta\delta$) is remarkably more pronounced for H2 than for H5 ($\Delta\delta$(H2) = 1.21 ppm vs $\Delta\delta$(H5) = 0.07 ppm). The reverse effect is observed upon coordination of the anionic imc ligand to a metal cation like Zn^{2+} because σ donation withdraws electron density from the ring. As shown by the **Zn-imc** spectrum, coordination mainly affects the signal corresponding to H2, which moves downfield with respect to the spectrum of imc ($\Delta\delta$(H2) = 0.48 ppm) while that associated with H5 remains nearly constant.

dx.doi.org/10.1021/ic502232v | *Inorg. Chem.* 2015, 54, 241−252

In the case of **1-SbZn**, the two-line spectrum shows behavior analogous to that described for the **Zn-imc** complex, i.e., the signal of H2 undergoes a significant downfield shift compared with the spectrum of imc while changes in the chemical shift of H5 are negligible. However, the signal of H2 in **1-SbZn** broadens, and its $\Delta\delta$ parameter becomes considerably larger ($\Delta\delta$(H2) = 0.90 ppm). This is most likely due to the mentioned intramolecular C−H···O_{POM} interaction, which promotes the deshielding of H2 and confers a characteristic spectrum on the **1-SbZn** species. No evidence of the presence of the free ligand or the Zn complex was observed. This indicates that **1-SbZn** remains stable upon dissolution and that no ligand dissociation occurs on the NMR time scale. The spectrum of **1-SbZn** remained unaltered for 5 days, showing that this hybrid POM does not undergo any significant structural transformation.

Analogous studies were also performed on our second diamagnetic species, and consistent results confirming the stability of **3-SbZn** in solution were obtained. This species also shows a distinct ^{1}H NMR spectrum that clearly differs from those of the free pyzc ligand in its acidic form and the **Zn-pyzc** complex[38] and remains unaltered for several days (Figure S9 in the Supporting Information). These results evidence that ^{1}H NMR spectroscopy is a suitable technique for analyzing the stability of diamagnetic POM organic derivatives, affording advantages in terms of time and sample consumption compared with other nuclei commonly used to evaluate the solution stability of polyoxotungstate frameworks.

CONCLUSIONS

This work affords further insight into the reactivity of the well-known family of Krebs-type sandwich POMs as it illustrates their potential for use in the preparation of molecular hybrid species under mild conditions via straightforward ligand replacement of labile water molecules on preformed or in situ-generated precursors. The first organic derivatives of 3d-metal-disubstituted Krebs-type POMs have been obtained using aromatic N,O-chelating anions as ligands. Seven hybrid tungstoantimonates with general formula $[\{M^{II}(L)(H_2O)\}_2(WO_2)_2(Sb^{III}W_9O_{33})_2]^{12-}$ have been isolated, namely, the series **1-SbM** (L = imc; M^{II} = Mn, Co, Ni, Zn), compound **2-SbNi** (L = pzc; M^{II} = Ni), and the pair **3-SbM** (L = pyzc; M^{II} = Co, Zn). Two $[\{M^{II}(imc)(H_2O)\}_2(WO_2)_2(Te^{IV}W_9O_{33})_2]^{10-}$ analogues (**1-TeM**, M^{II} = Mn, Co) with unprecedented 3d-metal-disubstituted Krebs-type tungstotellurate skeletons have also been obtained. Derivatization of Krebs-type POMs has proven to be extremely dependent on the specific nature of the ligand. For example, the imc anion has been identified as a "universal" ligand because it undergoes coordination regardless of the 3d metal or the reaction conditions, whereas the second diazolecarboxylate evaluated (pzc) either showed selectivity toward the functionalization of the Ni precursor or promoted partial decomposition of the Co analogue to give $[Co(pzc)_2(H_2O)_2]$ (**Co-pzc**). Selective behavior toward the Co and Zn precursors has also been observed for pyzc, but in contrast, the use of the other diazinecarboxylates (pydc and pymc) resulted in the corresponding $[M^{II}L_2(H_2O)_2]$ complexes (**Co-pydc**, **Ni-pydc**, and **Co-pymc**), while picolinate was found to be inert under all of the conditions tested. Functionalization can be efficiently monitored by IR spectroscopy, making this simple technique a powerful tool to establish the organic derivatization of the parent cluster prior to single-crystal X-ray diffraction. The hybrid species reported herein are stable in aqueous solution according to ^{1}H NMR studies performed on the diamagnetic **1-SbZn** and **3-SbZn** derivatives. We plan to extend these systematic studies to compositionally different Krebs-type anions and other model ligands to achieve better understanding of the reactivity of this POM family.

ASSOCIATED CONTENT

Supporting Information

Refinement details; TGA/DTA curves; FT-IR spectra; additional structural figures and tables; additional ^{1}H NMR spectra; full characterization of **M-pzc** (M = Co, Ni), **M-pydc** (M = Co, Ni), and **Co-pymc**; and X-ray crystallographic data for **1-SbM** (M = Mn, Co, Ni, Zn), **1-TeM** (M = Mn, Co, Ni), **2-SbNi**, **3-SbM** (M = Co, Zn), $[ZnSb_2]_\infty$, **M-pzc** (M = Co, Ni), and **Co-pymc** in CIF format. This material is available free of charge via the Internet at http://pubs.acs.org.

AUTHOR INFORMATION

Corresponding Authors

*E-mail: santiago.reinoso@ehu.es.
*E-mail: juanma.zorrilla@ehu.es.

Notes

The authors declare no competing financial interest.

ACKNOWLEDGMENTS

This work was funded by Eusko Jaurlaritza/Gobierno Vasco (EJ/GV) (Grants IT477-10 and S-PE13UN056), MINECO (Grant MAT2013-48366-C2-2-P), and Universidad del País Vasco/Euskal Herriko Unibertsitatea (UPV/EHU) (Grant UFI11/53). B.A. and A.P. thank EJ/GV for their predoctoral fellowships. Technical and human support provided by SGIker (UPV/EHU) is gratefully acknowledged.

REFERENCES

(1) (a) Pope, M. T. *Heteropoly and Isopoly Oxometalates*; Springer: Berlin, 1983. (b) *Polyoxometalates: From Platonic Solids to Anti-Retroviral Activity*; Pope, M. T., Müller, A., Eds.; Kluwer: Dordrecht, The Netherlands, 1994. (c) *Polyoxometalate Chemistry: From Topology via Self-Assembly to Applications*; Pope, M. T., Müller, A., Eds.; Kluwer: Dordrecht, The Netherlands, 2001. (d) *Polyoxometalate Chemistry for Nanocomposite Design*; Pope, M. T., Yamase, T., Eds.; Kluwer: Dordrecht, The Netherlands, 2002. (e) *Polyoxometalate Chemistry: Some Recent Trends*; Sécheresse, F., Ed.; World Scientific: Singapore, 2013.

(2) (a) Gouzerh, P.; Proust, A. *Chem. Rev.* **1998**, *98*, 77−111. (b) Proust, A.; Thouvenot, R.; Gouzerh, P. *Chem. Commun.* **2008**, 1837−1852. (c) Long, D.-L.; Tsunashima, R.; Cronin, L. *Angew. Chem., Int. Ed.* **2010**, *49*, 1736−1758. (d) Dolbecq, A.; Dumas, E.; Mayer, C. R.; Mialane, P. *Chem. Rev.* **2010**, *110*, 6009−6048.

(3) Proust, A.; Matt, B.; Villanneau, R.; Guillemot, G.; Gouzerh, P.; Izzet, G. *Chem. Soc. Rev.* **2012**, *41*, 7605−7622.

(4) For example, see: (a) Kortz, U.; Hussain, F.; Reicke, M. *Angew. Chem., Int. Ed.* **2005**, *44*, 3773−3777. (b) Boglio, C.; Micoine, K.; Derat, E.; Thouvenot, R.; Hasenknopf, B.; Thorimbert, S.; Lacôte, E.; Malacria, M. *J. Am. Chem. Soc.* **2008**, *130*, 4553−4561. (c) Piedra-Garza, L. F.; Dickman, M. H.; Moldovan, O.; Breunig, H. J.; Kortz, U. *Inorg. Chem.* **2009**, *48*, 411−413. (d) Joo, N.; Renaudineau, S.; Delapierre, G.; Bidan, G.; Chamoreau, L.-M.; Thouvenot, R.; Gouzerh, P.; Proust, A. *Chem.—Eur. J.* **2010**, *16*, 5043−5051. (e) Villanneau, R.; Racimor, D.; Messner-Henning, E.; Rousselière, H.; Picart, S.; Thouvenot, R.; Proust, A. *Inorg. Chem.* **2011**, *50*, 1164−1166. (f) Nomiya, K.; Togashi, Y.; Kasahara, Y.; Aoki, S.; Seki, H.; Noguchi, M.; Yoshida, S. *Inorg. Chem.* **2011**, *50*, 9606−9619.

(5) For example, see: (a) Kwen, H.; Young, V. G.; Maatta, E. A. *Angew. Chem., Int. Ed.* **1999**, *38*, 1145−1146. (b) Peng, Z. *Angew. Chem., Int. Ed.* **2004**, *43*, 930−935. (c) Pradeep, C. P.; Long, D.-L.; Newton, G. N.;

Song, Y.-F.; Cronin, L. *Angew. Chem., Int. Ed.* **2008**, *47*, 4388−4391. (d) Santoni, M.-P.; Pal, A. K.; Hanan, G. S.; Proust, A.; Hasenknopf, B. *Inorg. Chem.* **2011**, *50*, 6737−6745. (e) Li, D.; Song, J.; Yin, P.; Simotwo, S.; Bassler, A. J.; Aung, Y. Y.; Roberts, J. E.; Hardcastle, K. I.; Hill, C. L.; Liu, T. *J. Am. Chem. Soc.* **2011**, *133*, 14010−14016. (f) Tong, U. S.; Chen, W.; Ritchie, C.; Wang, X.; Song, Y.-F. *Chem.—Eur. J.* **2014**, *20*, 1500−1504.

(6) For example, see: (a) Chesnut, D. J.; Hagrman, D.; Zapf, P. J.; Hammond, R. P.; LaDuca, R., Jr.; Haushalter, R. C.; Zubieta, J. *Coord. Chem. Rev.* **1999**, *190−192*, 737−769. (b) Reinoso, S.; Vitoria, P.; Gutiérrez-Zorrilla, J. M.; Lezama, L.; San Felices, L.; Beitia, J. I. *Inorg. Chem.* **2005**, *44*, 9731−9742. (c) Lisnard, L.; Dolbecq, A.; Mialane, P.; Marrot, J.; Codjovi, E.; Sécheresse, F. *Dalton Trans.* **2005**, 3913−3920. (d) Jin, H.; Qi, Y.; Wang, E.; Li, Y.; Wang, X.; Qin, C.; Chang, S. *Cryst. Growth Des.* **2006**, *6*, 2693−2698. (e) Shi, D.-Y.; Zhao, J.-W.; Chen, L.-J.; Ma, P.-T.; Wang, J.-P.; Niu, J.-Y. *CrystEngComm* **2012**, *14*, 3108−3119. (f) Iturrospe, A.; San Felices, L.; Reinoso, S.; Artetxe, B.; Lezama, L.; Gutiérrez-Zorrilla, J. M. *Cryst. Growth Des.* **2014**, *14*, 2318−2328.

(7) For example, see: (a) Mialane, P.; Dolbecq, A.; Sécheresse, F. *Chem. Commun.* **2006**, 3477−3485. (b) Zhao, J.-W.; Li, B.; Zheng, S.-T.; Yang, G.-H. *Cryst. Growth Des.* **2007**, *7*, 2658−2664. (c) Liu, H.; Gómez-García, C. J.; Peng, J.; Sha, J.; Li, Y.; Yan, Y. *Dalton Trans.* **2008**, 6211−6218. (d) Liu, H.; Qin, C.; Wei, Y.-G.; Xu, L.; Gao, G.-G.; Li, F.-Y.; Qu, X.-S. *Inorg. Chem.* **2008**, *47*, 4166−4172. (e) Liu, H.; Gómez-García, C. J.; Peng, J.; Sha, J.; Wang, L.; Yan, Y. *Inorg. Chim. Acta* **2009**, *362*, 1957−1962.

(8) (a) Fang, X.; Anderson, T. M.; Hill, C. L. *Angew. Chem., Int. Ed.* **2005**, *44*, 3540−3544. (b) Zheng, S.-T.; Zhang, J.; Yang, G.-Y. *Angew. Chem., Int. Ed.* **2008**, *47*, 3909−3913. (c) Ritchie, C.; Boyd, T.; Long, D.-L.; Ditzel, E.; Cronin, L. *Dalton Trans.* **2009**, 1587−1592. (d) Belai, N.; Kapoor, P. N.; Dickman, M. H.; Butcher, R. J.; Pope, M. T. *Eur. J. Inorg. Chem.* **2009**, 5215−5218. (e) Rousseau, G.; Oms, O.; Dolbecq, A.; Marrot, J.; Mialane, P. *Inorg. Chem.* **2011**, *50*, 7376−7378.

(9) Bösing, M.; Loose, I.; Pohlmann, H.; Krebs, B. *Chem.—Eur. J.* **1997**, *3*, 1232−1237.

(10) Bi, L.-H.; Li, B.; Wu, L.-X. *Inorg. Chem. Commun.* **2008**, *11*, 1184−1186.

(11) (a) Bösing, M.; Nöh, A.; Loose, I.; Krebs, B. *J. Am. Chem. Soc.* **1998**, *120*, 7252−7259. (b) Rodewald, D.; Jeannin, Y. *C. R. Acad. Sci. Paris IIc* **1998**, *1*, 175−181. (c) Loose, I.; Droste, E.; Bösing, M.; Pohlmann, H.; Dickman, M. H.; Rosu, C.; Pope, M. T.; Krebs, B. *Inorg. Chem.* **1999**, *38*, 2688−2694. (d) Piepenbrink, M.; Limanski, E. M.; Krebs, B. *Z. Anorg. Allg. Chem.* **2002**, *628*, 1187−1191. (e) Liu, Y.-H.; Ma, P.-T.; Wang, J.-P. *J. Coord. Chem.* **2008**, *61*, 936−944.

(12) (a) Kortz, U.; Savelieff, M. G.; Bassil, B. S.; Keita, B.; Nadjo, L. *Inorg. Chem.* **2002**, *41*, 783−789. (b) Limanski, E. M.; Drewes, D.; Droste, E.; Böhner, R.; Krebs, B. *J. Mol. Struct.* **2003**, *656*, 17−25. (c) Hussain, F.; Reicke, M.; Janowski, V.; de Silva, S.; Futuwi, J.; Kortz, U. *C. R. Chim.* **2005**, *8*, 1045−1056. (d) Wang, J.-P.; Ma, P.-T.; Li, J.; Niu, H.-Y.; Niu, J.-Y. *Chem.—Asian J.* **2008**, *3*, 822−833. (e) Carraro, M.; Bassil, B. S.; Sorarù, A.; Berardi, S.; Suchopar, A.; Kortz, U.; Bonchio, M. *Chem. Commun.* **2013**, *49*, 7914−7916.

(13) (a) Laurencin, D.; Villanneau, R.; Herson, P.; Thouvenot, R.; Jeannin, Y.; Proust, A. *Chem. Commun.* **2005**, 5524−5526. (b) Bi, L.-H.; Al-Kadamany, G.; Chubarova, E. V.; Dickman, M. H.; Chen, L.; Gopala, D. S.; Richards, R. M.; Keita, B.; Nadjo, L.; Jaensch, H.; Mathys, G.; Kortz, U. *Inorg. Chem.* **2009**, *48*, 10068−10077. (c) Zhang, L.-C.; Xue, H.; Zhu, Z.-M.; Wang, Q.-X.; You, W.-S.; Li, Y.-G.; Wang, E.-B. *Inorg. Chem. Commun.* **2010**, *13*, 609−612. (d) Kalinina, I. V.; Izarova, N. V.; Kortz, U. *Inorg. Chem.* **2012**, *51*, 7442−7444. (e) Zhao, C.; Kambara, C. S.; Yang, Y.; Kaledin, A. L.; Musaev, D. G.; Lian, T.; Hill, C. L. *Inorg. Chem.* **2013**, *52*, 671−678. (f) Ismail, A. H.; Bassil, B. S.; Römer, I.; Kortz, U. *Z. Anorg. Allg. Chem.* **2013**, *639*, 2510−2515.

(14) (a) Bonchio, M.; Carraro, M.; Scorrano, G.; Kortz, U. *Adv. Synth. Catal.* **2005**, *347*, 1909−1912. (b) Bonchio, M.; Carraro, M.; Sartorel, A.; Scorrano, G.; Kortz, U. *J. Mol. Catal. A: Chem.* **2006**, *251*, 93−99. (c) Sartorel, A.; Carraro, M.; Scorrano, G.; Bassil, B. S.; Dickman, M. H.; Keita, B.; Nadjo, L.; Kortz, U.; Bonchio, M. *Chem.—Eur. J.* **2009**, *15*, 7854−7858. (d) Evangelisti, F.; Car, P.-E.; Blacque, O.; Patzke, G. R. *Catal. Sci. Technol.* **2013**, *3*, 3117−3129.

(15) (a) Bi, L.-H.; Li, B.; Bi, S.; Wu, L.-X. *J. Solid State Chem.* **2009**, *182*, 1401−1407. (b) Bi, L.-H.; Hou, G.-F.; Bao, Y.-Y.; Li, B.; Wu, L.-X.; Gao, Z.-M.; McCormac, T.; Mal, S. S.; Dickman, M. H.; Kortz, U. *Eur. J. Inorg. Chem.* **2009**, 5259−5266.

(16) Dolbecq, A.; Compain, J.-D.; Mialane, P.; Marrot, J.; Rivière, E.; Sécheresse, F. *Inorg. Chem.* **2008**, *47*, 3371−3378.

(17) *CrysAlisPro Software System*; Agilent Technologies UK Ltd.: Oxford, U.K., 2012.

(18) Dolomanov, O. V.; Bourhis, L. J.; Gildea, R. J.; Howard, J. A. K.; Puschmann, H. *J. Appl. Crystallogr.* **2009**, *42*, 339−341.

(19) Sheldrick, G. M. *Acta Crystallogr.* **2008**, *A64*, 112−122.

(20) Spek, A. L. *Acta Crystallogr.* **2009**, *D65*, 148−155.

(21) Farrugia, L. J. *J. Appl. Crystallogr.* **1999**, *32*, 837−838.

(22) Brown, I. D.; Altermatt, D. *Acta Crystallogr.* **1985**, *B41*, 244−247.

(23) Alvarez, S.; Alemany, P.; Casanova, D.; Cirera, J.; Llunell, M.; Avnir, D. *Coord. Chem. Rev.* **2005**, *249*, 1693−1708.

(24) Llunell, M.; Casanova, D.; Cirera, J.; Bofill, J. M.; Alemany, P.; Alvarez, S.; Pinsky, M.; Avnir, D. *SHAPE*, version 1.1b; Universitat de Barcelona: Barcelona, Spain and The Hebrew University of Jerusalem: Jerusalem, Israel, 2005.

(25) Kortz, U.; Al-Kassem, N. K.; Savelieff, M. G.; Al Kadi, N. A.; Sadakane, M. *Inorg. Chem.* **2001**, *40*, 4742−4749.

(26) **$K_{2.4}Na_{7.6}[\{Ni^{II}(imc)(H_2O)\}_2(WO_2)_2(Te^{IV}W_9O_{33})_2]\cdot 40H_2O$ (1-TeNi).** IR (cm^{-1}): 1582(m), 1503(w), 1435(w), 1391(m), 1240(w), 1225(w), 1092(w), 962(s), 843(vs), 781(s), 741(w), 689(m), 658(m), 513(w). Crystal data: $C_8H_{90}K_{2.4}N_4Na_{7.6}Ni_2O_{116}Te_2W_{20}$, fw = 6417.0 g mol^{-1}, triclinic, $P\bar{1}$ space group, a = 12.9079(4) Å, b = 15.4074(5) Å, c = 16.0861(5) Å, α = 63.706(3)°, β = 71.705(3)°, γ = 77.412(3)°, V = 2711.5(2) $Å^3$, T = 100(2) K, Z = 1, D_{calcd} = 3.926 g cm^{-3}, μ = 22.234 mm^{-1}, 18 192 reflections collected, 10 634 unique (R_{int} = 0.033), 9555 observed [$I > 2\sigma(I)$], 396 parameters, $R(F)$ = 0.042 [$I > 2\sigma(I)$], $wR(F^2)$ = 0.106 (all data), GOF = 1.065.

(27) Zheng, S.; Cai, S.; Fang, J.; Zhang, W. *Acta Crystallogr.* **2011**, *E67*, m865.

(28) **$[M^{II}(pzc)(H_2O)_2]$, M^{II} = Co (Co-pzc), Ni (Ni-pzc).** Synthesis: To a solution of $MCl_2\cdot 6H_2O$ (M = Co, Ni; 71 mg; 0.30 mmol) in hot water (15 mL) was added 1*H*-pyrazole-3-carboxylic acid (74 mg, 0.60 mmol) dissolved in hot water (10 mL) dropwise. After 30 min of stirring at 90 °C, the final solution was cooled to room temperature and left to evaporate in an open container. Crystals suitable for X-ray diffraction were obtained after a few days. **Co-pzc**: Yield: 51 mg, 54%. Anal. Calcd (Found) for $C_8H_{10}CoN_4O_6$: C, 30.30 (30.86); H, 3.18 (3.21); N, 17.67 (17.39). IR (cm^{-1}): 1604(vs), 1518(m), 1497(m), 1442(m), 1362(vs), 1244(s), 1180(m), 1115(m), 1074(m), 1001(m), 928(m), 897(m), 835(m), 770(m), 698(m), 613(m), 492(m). Crystal data: $C_8H_{10}CoN_4O_6$, fw = 317.1 g mol^{-1}, monoclinic, $P2_1/c$ space group, a = 5.0874(1) Å, b = 11.4002(3) Å, c = 9.2880(4) Å, β = 96.932(2)°, V = 534.74(2) $Å^3$, T = 100(2) K, Z = 2, D_{calcd} = 1.970 g cm^{-3}, μ = 1.639 mm^{-1}, 4004 reflections collected, 1110 unique (R_{int} = 0.024), 1025 observed [$I > 2\sigma(I)$], 94 parameters, $R(F)$ = 0.023 [$I > 2\sigma(I)$], $wR(F^2)$ = 0.056 (all data), GOF 1.079. **Ni-pzc**: Yield: 63 mg, 66%. Anal. Calcd (Found) for $C_8H_{10}N_4NiO_6$: C, 30.32 (29.40); H, 3.18 (3.35); N, 17.68 (16.99). IR (cm^{-1}): 1616(s), 1518(m), 1497(m), 1443(m), 1364(s), 1244(m), 1182(m), 1117(m), 1078(m), 1005(w), 930(w), 899(w), 851(m), 839(m), 772(m), 693(m), 613(m), 494(w). Crystal data: $C_8H_{10}N_4NiO_6$, fw = 316.9 g mol^{-1}, monoclinic, $P2_1/c$ space group, a = 5.0879(3) Å, b = 11.2855(6) Å, c = 9.2686(6) Å, β = 97.216(6)°, V = 527.99(6) $Å^3$, T = 100(2) K, Z = 2, D_{calcd} = 1.993 g cm^{-3}, μ = 3.031 mm^{-1}, 2552 reflections collected, 893 unique (R_{int} = 0.024), 791 observed [$I > 2\sigma(I)$], 96 parameters, $R(F)$ = 0.024 [$I > 2\sigma(I)$], $wR(F^2)$ = 0.063 (all data), GOF 1.077.

(29) López-Viseras, M. E.; Fernández, B.; Hilfiker, S.; Sánchez González, C.; Llopis González, J.; Calahorro, A. J.; Colacio, E.; Rodríguez-Diéguez, A. *J. Inorg. Biochem.* **2014**, *131*, 64−67.

(30) Artetxe, B.; Reinoso, S.; San Felices, L.; Martín-Caballero, J.; Gutiérrez-Zorrilla, J. M. *Acta Crystallogr.* **2013**, *E69*, m420−m421.

(31) $[M^{II}(pydc)(H_2O)_2]\cdot 2H_2O$, M^{II} = Co (**Co-pydc**), Ni (**Ni-pydc**). Synthesis: The synthetic procedure for **M-pzc** was followed, except that pyridazine-3-carboxylic acid (74 mg, 0.60 mmol) was used. **Co-pydc**: Yield: 97 mg, 86%. Anal. Calcd (Found) for $C_{10}H_{14}CoN_4O_8$: C, 31.84 (31.35); H, 3.74 (3.48); N, 14.85 (14.41). IR (cm^{-1}): 1626(s), 1580(m), 1559(s), 1451(w), 1385(w), 1163(w), 1090(w), 1074(w), 988(m), 851(m), 783(m), 721(m), 675(m). **Ni-pydc**: Yield: 81 mg, 72%. Anal. Calcd (Found) for $C_{10}H_{14}N_4NiO_8$: C, 31.86 (32.27); H, 3.74 (3.64); N, 14.86 (14.94). IR (cm^{-1}): 1628(s), 1580(m), 1560(s), 1454(w), 1385(w), 1163(w), 1092(w), 1078(w), 988(m), 851(m), 783(m), 725(m), 669(m).

(32) $[Co^{II}(pymc)(H_2O)_2]\cdot 2H_2O$ (**Co-pymc**). Synthesis: The synthetic procedure for **Co-pzc** was followed, except that pyrimidine-4-carboxylic acid (74 mg, 0.60 mmol) was used. Yield: 58 mg, 51%. Anal. Calcd (Found) for $C_{10}H_{14}CoN_4O_8$: C, 31.84 (31.70); H, 3.74 (3.68); N, 14.85 (14.73). IR (cm^{-1}): 1626(s), 1595(s), 1557(s), 1402(s), 1383(s), 1304(m), 1207(w), 1173(w), 1155(w), 1074(m), 1026(m), 860(m), 810(m), 712(m), 619(w), 542(w), 436(w). Crystal data: $C_{10}H_{14}CoN_4O_8$, fw = 377.18 g mol^{-1}, triclinic, $P\bar{1}$ space group, a = 5.5524(5) Å, b = 7.1608(8) Å, c = 9.4616(9) Å, α = 81.680(9)°, β = 88.202(8)°, γ = 70.571(9)°, V = 350.98(6) $Å^3$, T = 100(2) K, Z = 1, D_{calcd} = 1.785 g cm^{-3}, μ = 1.274 mm^{-1}, 2166 reflections collected, 1380 unique (R_{int} = 0.024), 1241 observed [$I > 2\sigma(I)$], 117 parameters, $R(F)$ = 0.032 [$I > 2\sigma(I)$], $wR(F^2)$ = 0.068 (all data), GOF 1.024.

(33) Aakeröy, C. B.; Desper, J.; Levin, B.; Valdés-Martínez, J. *Inorg. Chim. Acta* **2006**, *359*, 1255−1262.

(34) $K_4Na_6[\{Zn^{II}(H_2O)_2\}_{1.4}\{WO(OH)_2\}_{0.6}(Sb^{III}_2W_{20}O_{70})]\cdot 30H_2O$ ($[ZnSb_2]_\infty$). IR (cm^{-1}): 949(s), 901(s), 868(s), 806(vs), 745(s), 648(m), 513(w), 432(w). Crystal data: $H_{66.8}K_4Na_6O_{104.6}Sb_2W_{20.6}Zn_{1.4}$, fw = 6157.6 g mol^{-1}, monoclinic, $C2/c$ space group, a = 23.7929(4) Å, b = 22.7751(3) Å, c = 19.6239(3) Å, β = 110.799(2)°, V = 9940.9(3) $Å^3$, T = 100(2) K, Z = 4, D_{calcd} = 4.114 g cm^{-3}, μ = 24.905 mm^{-1}, 27 292 reflections, 9774 unique (R_{int} = 0.040), 8799 observed [$I > 2\sigma(I)$], 359 parameters, $R(F)$ = 0.039 [$I > 2\sigma(I)$], $wR(F^2)$ = 0.098 (all data), GOF = 1.056.

(35) Chen, B.-W.; Chen, W.-L.; Li, Y.-G.; Wang, E.-B. *J. Cluster Sci.* **2011**, *22*, 73−85.

(36) San Felices, L.; Vitoria, P.; Gutiérrez-Zorrilla, J. M.; Lezama, L.; Reinoso, S. *Inorg. Chem.* **2006**, *45*, 7748−7757.

(37) Artetxe, B.; San Felices, L.; Pache, A.; Reinoso, S.; Gutiérrez-Zorrilla, J. M. *Acta Crystallogr.* **2013**, *E69*, m94.

(38) Ptasiewicz-Bak, H.; Leciejewicz, J.; Zachara, J. *J. Coord. Chem.* **1995**, *36*, 317−326.

(39) Shuai, W.; Cai, S.; Zheng, S. *Acta Crystallogr.* **2011**, *E67*, m897.